Chapter 17
Analysis of Metallic Plume Image Characteristics During High Power Disk Laser Welding

Xiangdong Gao, Runlin Wang, Yingying Liu and Yongchen Yang

Abstract Metallic plume is an important phenomenon during high power disk laser deep-penetration welding, which can reflect the welding quality. To study this laser-induced plume characteristics and its relation to welding quality, an extraviolet and visible sensitive high speed color camera was used to capture the metallic plumes in a high-power disk laser bead on plate deep-penetration welding of Type 304 austenitic stainless steel plates at a continuous laser power of 10 kW. These captured digital images were firstly processed in RGB color spaces, and then were transferred to the Hue-Saturation-Intensity (HSI) color spaces from the RGB color spaces. The area of metallic plume was segmented and defined as the plume eigenvalue. The fluctuation of weld bead width was used to evaluate the welding stability. To monitor the plume behavior, a short-time Fourier transform was applied to obtain the time–frequency characteristics of plume images. Also, the hierarchical clustering was analyzed for the time–frequency characteristics of plume images. The results of hierarchical clustering showed there existed relationship between the metallic plume area and welding quality, and the fitting curve of clustering could reflect the fluctuation trend of the weld bead width effectively.

Keywords Disk laser welding · Hierarchical clustering · Image characteristics · Metallic plume image · Short-time Fourier transform · Time–frequency analysis

X. Gao (✉) · R. Wang · Y. Liu · Y. Yang
School of Electromechanical Engineering, Guangdong University of Technology, 510006 Guangzhou, China
e-mail: gaoxd666@126.com

R. Wang
e-mail: xdgao@hotmail.com

Y. Liu
e-mail: liu15045105965@126.com

Y. Yang
e-mail: gaoxd@gdut.edu.cn

H. K. Kim et al. (eds.), *IAENG Transactions on Engineering Technologies*, Lecture Notes in Electrical Engineering 247, DOI: 10.1007/978-94-007-6818-5_17,

17.1 Introduction

High power disk laser welding is a competitive welding method and is well known for its high welding speed, good welding quality and deep penetration. In recent years, the disk laser welding has been widely used in automotive production and electronic industry. During a high power disk laser welding, a metallic plume mixture is generated quickly from the surface of the welded material. This plume mainly consists of the metal vapor and is one of the most important phenomenon which can be used to monitor the laser welding quality. Research works have shown that the metallic plume has negative effects on the energy transference efficiency of the laser beam and the welding quality [1, 2]. There exists an internal relationship between the plume characteristics and the welding status. To monitor and control the welding quality in real-time, it is necessary to investigate the metallic plume characteristics and its influences upon the weld quality.

In recent years, some researches such as spectroscopy, photoelectric signal processing, acoustic signal processing, vision methods, and so on were performed to study the dynamic behaviors of the metallic plume [3–6]. The holographic interferometry was applied to study the laser-induced plume [7]. The Fourier transform was used to analyze the acoustic signal of metal vapor and the time–frequency was applied to study the plasma characteristics [8, 9]. These study results showed that the density and the size of the plasma were related to the laser power and beam focus position. There were relations between the metallic plume and the weld quality. However, it is still difficult to find the exact relationship between the characteristics of metallic plume and the weld quality.

In order to obtain more detailed dynamic information about metallic plume, the high-speed photography was used to record the color images of metallic plume in a high power disk laser welding process. High-speed photography is an effective method and is widely used in the welding process, it can accurately capture and monitor the instant information of metallic plume. The important characteristic features of plumes could be extracted from these color images [10, 11]. Usually, the more energy a weldment absorbs, the bigger the metallic plume is. Here, the metallic plume area was used as the characteristic parameters, and the short-time Fourier transform was applied to the area of metallic plume to obtain the time–frequency characteristics of plume. Also, the hierarchical clustering was used to analyze the plume characteristics and finally the clustering curves of metallic plume area were plotted. Welding experimental results showed that in a definite parameter combination, the 6th fitting curves of the metallic plume area frequency characteristic clustering could effectively reflect the fluctuation trend of the weld bead width.

17.2 Experimental Apparatus and Plume Characteristic Extraction

17.2.1 Experimental Apparatus

The schematic of a disk laser welding experimental apparatus is shown in Fig. 17.1. The experimental system consisted of a TruDisk-10003 disk laser welding equipment (laser power 10 kW), a Motoman 6-axis robot and a welding experimental platform equipped with shielding gas (argon), servo motors and fixing devices. An extraviolet and visible sensitive high speed color camera was used to capture the metallic plume dynamic color images during a 10 kW high-power bead-on-plate disk laser welding. The welding conditions are listed in Table 17.1

17.2.2 Extraction of Plume Characteristics in RGB Space

The high-speed camera collected 2,400 frames RGB image of the metallic plume within 1.2 s, and each frame image corresponded to a welding status. The top view of a welded specimen is shown in Fig. 17.2. It can be seen that the middle part of

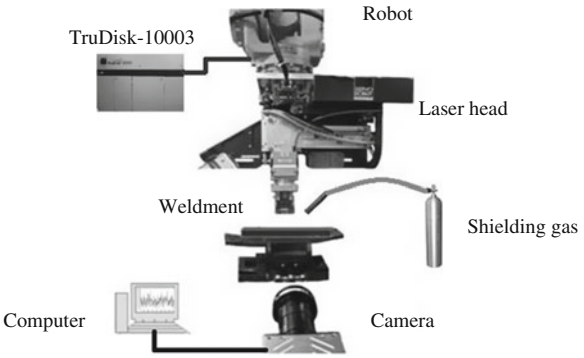

Fig. 17.1 Experimental apparatus of high power disk laser welding

Table 17.1 Welding experimental conditions

Welding apparatus	TruDisk-10003
Laser power	10 kW
Spot diameter	480 μm
Laser wavelength	1,030 nm
Welding speed	4.5 m/min
Camera speed	2,000 frame/s
Image resolution	512 × 512 pixel
Size of weldment	150 × 100 × 10 mm
Weldment	Type 304 austenitic stainless steel

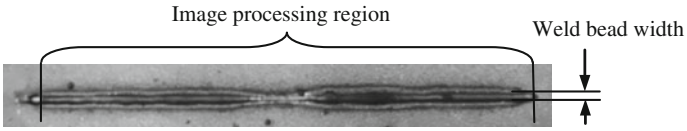

Fig. 17.2 *Top* view of a welded specimen of high-power disk laser welding

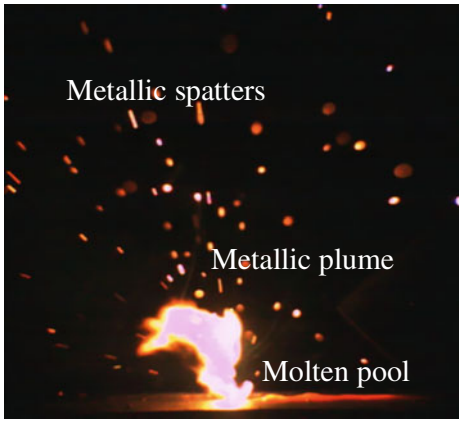

Fig. 17.3 Original metallic plume color image

the weld seam is narrow and has poor quality. This region corresponded to 1,066–1,333 frame images. The captured plume images from 481 to 2,400 frames were processed to study their characteristics. An original metallic plume color image is shown in Fig. 17.3. It can be seen that the captured image includes the information of metallic spatters, metallic plume and molten pool.

When the disk laser beam focused on a weldment, the laser energy was transfered to the surface of weldment, the weldment melted immediately and the metallic plume emerged. The area of metallic plume could reflect the absorptivity of laser energy which reflected the welding quality. Thus, the metallic plume area could be used as a characteristic parameter. In order to extract the plume characteristics accurately and reduce calculation, metallic plume were tailored from an original color image. The tailored RGB image is shown in Fig. 17.4.

The tailored plume image was turned to gray scale image. Due to random interference signals in the welding, there were a lot of noises in the image when it was recorded, the filtering was used to eliminate these noises. Commonly used filtering methods are frequency filtering and spatial filtering. This experiment used the spatial filtering to deal with the noises. Spatial filtering can be divided into linear filtering and nonlinear filtering. Linear filtering is also called as mean filtering, and is a low pass filter. Because the profile of image edge contains a lot of high frequency information, so the boundary of image becomes fuzzy by using the mean filtering eliminating the noises. Boundary is one of the most basic image features and often carries much image information that is of great importance in analyzing, describing and understanding an image.

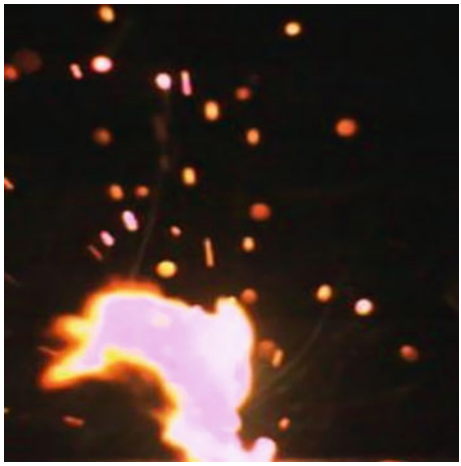

Fig. 17.4 Tailored *RGB* image of metallic plume

Wiener filtering and Median filtering are commonly used for nonlinear filtering and they can not only filter all kinds of noises, but also protect the boundary information such as edge and sharp corner. Wiener filtering characterized by the feature of good recovery effect, low computation and good performance of noise reduction, are widely used in image recovery. Wiener filtering was used in this experiment. The experiment applied a group of filtering windows to conduct the Wiener filtering processing, and the results are shown in Fig. 17.5. It is observed from Fig. 17.5 that the filtering effect of 35 × 35 filtering window is best. It also can be seen from Fig. 17.5c that the noises such as spatter, halo and so on were filtered by Wiener filtering, the edge information was protected and the images were clear.

Image segmentation is of importance in image processing. The accuracy of image segmentation has a direct influence on the subsequent image refining and recognition results. Image segmentation is based on the edge, shape, gray value and position to divide an image into different kinds of regions, and separates the target image from background. The commonly used method of image segmentation is threshold segmentation such as image binarization. When the gray scale of target is greatly different from background and the layers of image are clear, threshold segmentation can better detect the target. Threshold segmentation can not only compress the data quantity, but also simplify the analysis and processing steps. Therefore, in many cases, it is an indispensable image preprocessing process, feature extraction and pattern recognition. Threshold segmentation method principle can be described as follows. Lets an original grayscale image is $f(x,y)$, then a gray value T of original grayscale image $f(x,y)$ can be found with some certain criteria to divide image into two parts. The divided binary image is given by

$$g(x,y) = \begin{cases} a & f(x,y) \geq T \\ b & f(x,y) < T \end{cases} \tag{17.1}$$

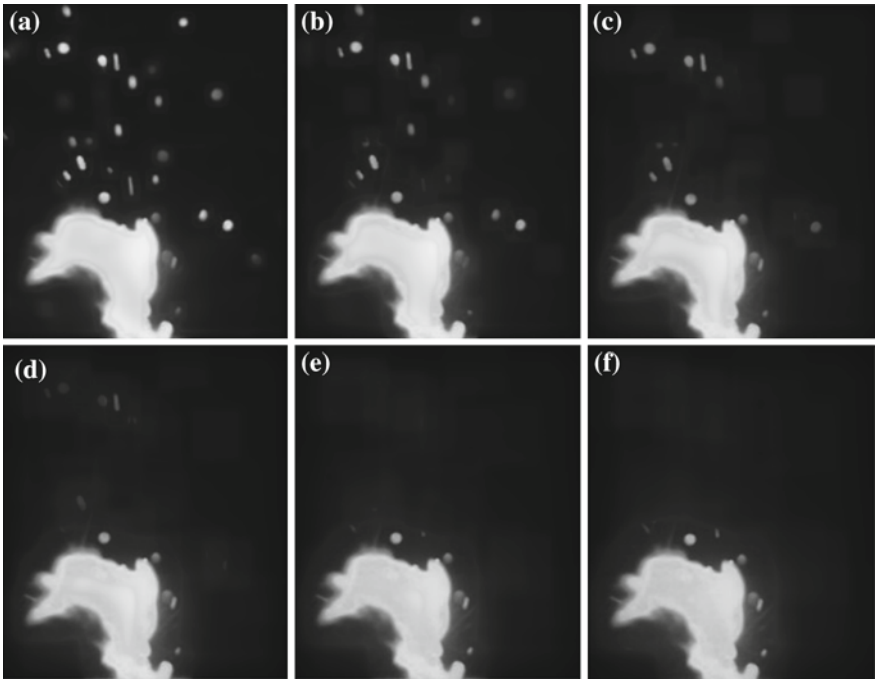

Fig. 17.5 Effect diagram of Wiener filter. **a** 15 × 15 filtering window. **b** 25 × 25 filtering window. **c** 35 × 35 filtering window. **d** 45 × 45 filtering window. **e** 55 × 55 filtering window. **f** 65 × 65 filtering window

The image belonging to different target region is defined by threshold value, so the selection of optimal threshold T is the key for deciding the effect of threshold segmentation. If the threshold value is too high, overmuch target points are classified as the background falsely. If the threshold value is too low, the opposite situation appears. Commonly used threshold selection method is P—tile method, Otsu method, average gray method, the waterline threshold method, the maximum entropy method and fuzzy set method and so on. Owing to the complex algorithm, the latest methods like the maximum entropy method and fuzzy set method are not applicable to this experiment. P—tile method, Otsu method, average gray method and the waterline threshold method are applied and the results are shown in Fig. 17.6. It can be observed from Fig. 17.6 that the size and morphology of the metallic plume is the same with the Otsu image and it could meet the computing requirement. After image segmentation, there were a lot of spatters in some metallic plume images, and this would influence the extraction of plume characteristics, so the image areas with less than 200 pixels were deleted and the final metallic plume images could be obtained.

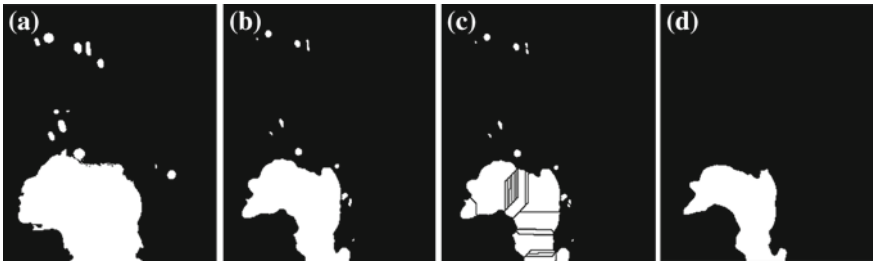

Fig. 17.6 Image segmentation of laser-induced metallic plumes. **a** Average gray method. **b** P—tile method. **c** Waterline threshold method. **d** Otsu method

17.2.3 Extraction of Plume Characteristics in HSI Space

Color space has many description including RGB color spaces, HIS color space plays an important role in image analysis. HSI color space uses the hue, saturation and intensity to describe colors which have a better performance in scenery cognitive than RGB color spaces. Here we used HSI method to process the plume images. An original RGB image of metallic plume shown in Fig. 17.4 was tailored. Then this tailored RGB image of metallic plume was converted to the HSI image and is shown in Fig. 17.7. Respectively, H component, S component and I component could be obtained from the mathematical formulas. H component is given by

$$H = \begin{cases} \theta & if \quad B \leq G \\ 360 - \theta & if \quad B > G \end{cases} \tag{17.2}$$

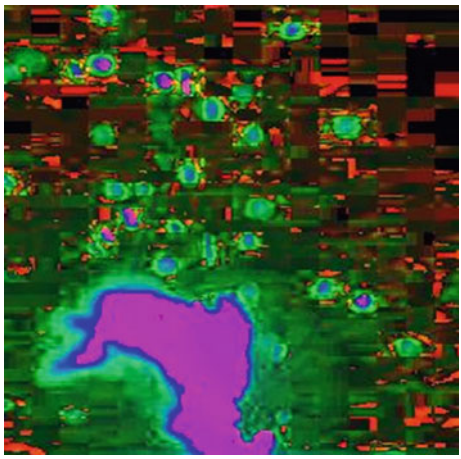

Fig. 17.7 HSI image of metallic plume

where

$$\theta = \arccos\left\{\frac{\frac{1}{2}[(R-G)+(R-B)]}{[(R-G)^2+(R-B)(G-B)]^{1/2}}\right\} \tag{17.3}$$

S component is given by

$$S = 1 - \frac{3}{(R+G+B)}[\min(R,G,B)] \tag{17.4}$$

I component is given by

$$I = \frac{1}{3}(R,G,B) \tag{17.5}$$

where R, G, B are three components of RGB color spaces.

H component image, S component image and I component image are shown in Fig. 17.8. The central part of metallic plume absorbs more laser energy and has a key influence on laser beam and welding. H component reflects the central part of metallic plume which can be used to extract the plume characteristics. In the H component image, the body of metallic plume is obviously different from black background. The Otsu threshold segmentation was used to segment the metallic plume. Setting global threshold 200 could remove the white spots and the metallic plume was segmented. It can be observed that the segmented metallic plume contains several small black holes. Through filling these holes, the final metallic plume is achieved. The image processing procedure of metallic plume is shown in Fig. 17.9. The plume area of whole metallic plume images were calculated, as shown in Fig. 17.10.

The metallic plume area was used to study the plume characteristics. In this experiment, the image processing methods of both RGB spaces and HSI spaces were available, and from the curves it is difficult to find there existed the obvious fluctuations of metallic plume area. Therefore, we considered applying the

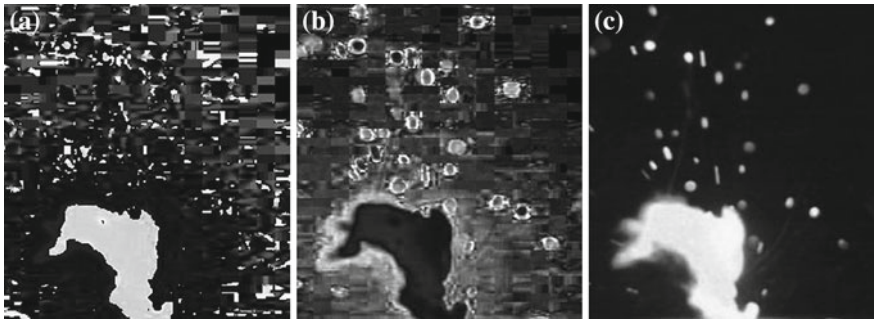

Fig. 17.8 **a** H component image. **b** S component image and **c** I component image of metallic plume

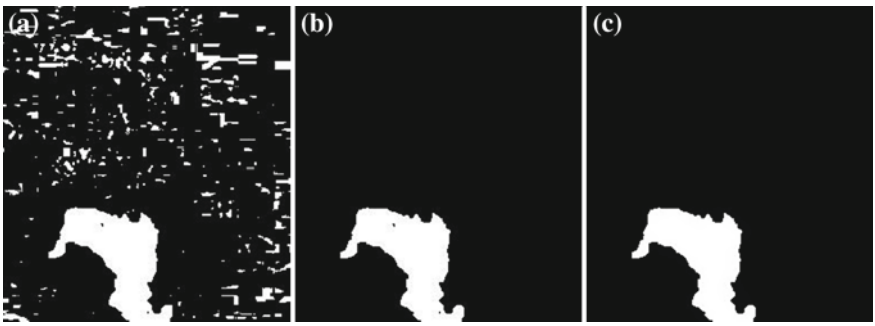

Fig. 17.9 Schematic diagram of metallic plume image processing. **a** Binary image. **b** Segmented image. **c** Final image

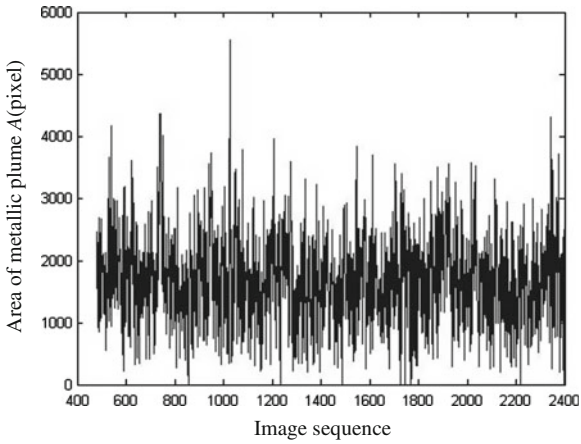

Fig. 17.10 *Curves* of metallic plume area with Image sequences

methods of short-time Fourier transform and hierarchical clustering to investigate the plume characteristics in HSI color spaces.

17.3 Short-Time Fourier Transform

17.3.1 Concept of Short-Time Fourier Transform

Short-time Fourier transform (STFT) can not only reflect the time-domain feature of signals, but also present the spectrum of signals clearly. Its basic idea is that the signal to be transformed is multiplied by a limited window function before the Fourier transform is applied, and this window function is nonzero for only a short period of time. This window slides along the time axis, resulting in a two-dimensional representation of the signal. This can be mathematically written as [12]

$$STFT_Z(t,f) = \int_{-\infty}^{\infty} z(t)\eta^*(t-t')e^{-j2\pi ft}dt \tag{17.6}$$

where $z(t)$ is the signal to be transformed and $\eta^*(t-t')$ is the window function around t'. Through $z(t)\eta^*(t-t')$, the signal around t' is obtained and the short-time Fourier transform is just the Fourier transform of $z(t)\eta^*(t-t')$.

17.3.2 Window Function

The frequently-used window functions are Rectangular window, Gauss window, Hanning window, Hamming window, Blackman window, Triangle window, Cosine slope window, Index window and Bartlett-Hanning window. In welding experiment, Gauss window, Hanning window, Hamming window and Bartlett-Hanning window were applied to the short-time Fourier transform.

Suppose $x(n)$ is the signal sequence and $w(n)$ is a window function whose length is N. The expression of the Gauss window is

$$w(n) = e^{-\frac{1}{2}\left(\frac{n-(N-1)/2}{\sigma(N-1)/2}\right)^2} \tag{17.7}$$

where $\sigma \leq 0.5$.

The expression of the Hanning window is

$$w(n) = 0.5 - \left(1 - \cos\left(\frac{2\pi n}{N-1}\right)\right) \tag{17.8}$$

The expression of the Hamming window is

$$w(n) = 0.53 - 0.46\cos\left(\frac{2\pi n}{N-1}\right) \tag{17.9}$$

The expression of the Bartlett-Hanning window is

$$w(n) = 0.42 - 0.5\cos\left(\frac{2\pi n}{N-1}\right) + 0.08\cos\left(\frac{4\pi n}{N-1}\right) \tag{17.10}$$

In order to improve the temporal resolution of short-time Fourier transform, the length of window function should be as short as possible. At the same time, in order to get a higher frequency resolution, the length of the window should be as long as possible. In practical application, the length of the window function should be adapted to the length of signal local smooth length [13]. In laser welding experiment, the numerical values of length were set to be 64, 128, 256, respectively.

17.3.3 Analysis of Short-Time Fourier Transform

In short-time Fourier transform, the different window types, different window length and different step length were chosen. The detailed combination parameters are listed in Table 17.2.

Using the short-time Fourier transform, $4 \times 3 \times 3 = 36$ groups of data were obtained, in which the numbers of window types, length, step length were 4, 3, 3, respectively. Taking a group of data for example, the parameters were Gauss, 64, 10. The window length was 64 and it slid along the time axis 186 times during the short-time Fourier transform, so this group of data was a matrix whose size was 64×186. Figure 17.11 is a 3-D map of time–frequency information and Fig. 17.12 is the contour map of time–frequency.

As mentioned above, the image sequence 1,066–1,333 frames corresponded to the middle part of the weld bead. This region of weld bead was narrow and had poor quality. Observing Figs. 17.11 and 17.12, there were not obvious characteristics of 1,066–1,333 frames. For further study, the 50th, 70th, 110th frequency curves were extracted to analyze their characteristics. These three groups of data corresponded to three vertical lines, shown in Fig. 17.12. Figure 17.13 shows these three frequency curves.

To distinguish these three frequency curves more effectively, their numerical values of average, maximum, minimum, range, interquartile range (IQR), standard deviation and sum were calculated. The range was what the biggest number minus the smallest number. The IQR is the distance between the 75th percentile and the 25th percentile. The expression of standard deviation is

Table 17.2 Combination parameters of short-time Fourier transform

Window types	Gauss, Hanning, Hamming, Bartlett-Hanning
Length	64, 128, 256
Step length	1, 5, 10

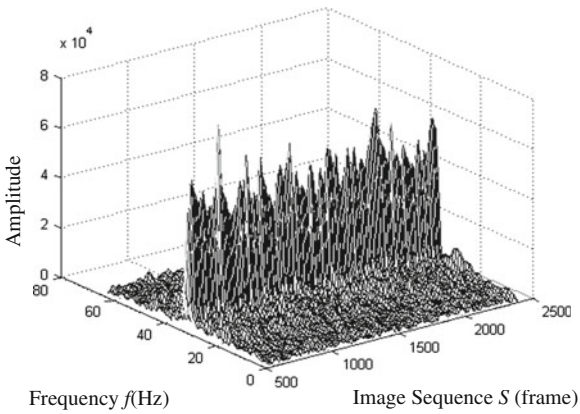

Fig. 17.11 3-D Map of time–frequency of plume area. Frequency f(Hz)

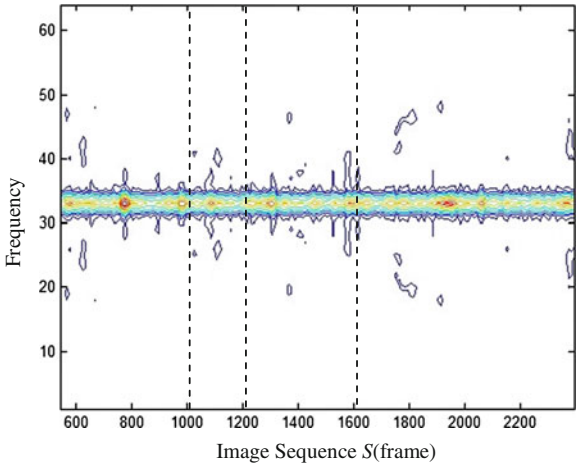

Fig. 17.12 Contour map of time–frequency of plume area

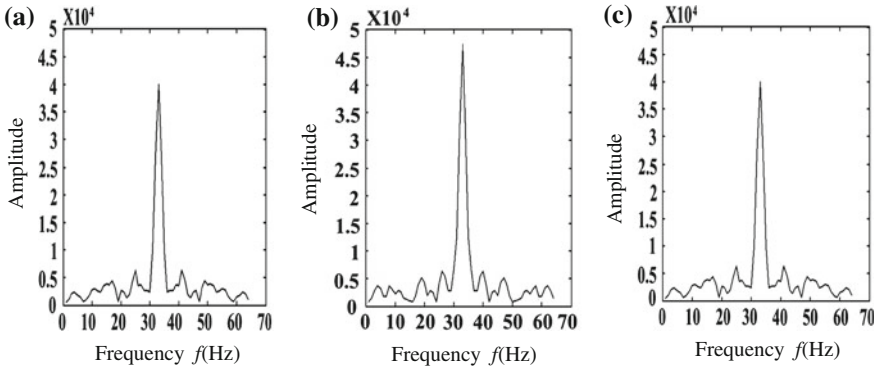

Fig. 17.13 Curves of the 50th, 70th, 110th frequency of plume area signals. **a** The 50th group of data. **b** The 70th group of data. **c** The 110th group of data

$$s = \left(\frac{1}{n-1} \sum_{i=1}^{n} (x_i - \bar{x})^2 \right)^{1/2} \quad i = 1, 2, 3 \ldots n \tag{17.11}$$

where $\bar{x}$ is the average value. All these eigenvalues are listed in Table 17.3.

It was found from Fig. 17.13 that three frequency curves had similar shapes. These three curves could be distinguished from Table 17.3 effectively by seven eigenvalues. Thus, these seven eigenvalues could represent different spectrum curves at any time. Also, we used the statistical method to calculate all frequency curve eigenvalues and analyze them by the Hierarchical clustering.

Table 17.3 Eigenvalues of different curves among Fig. 17.13 (unit:a.u)

	Fig. 17.13a	Fig. 17.13b	Fig. 17.13c
Max value	39,922	47,275	42,242
Min value	573	815	107
Average	4,199	4,840	3,787
IQR	1,893	2,318	2,825
Range	39,348	46,459	42,134
Standard deviation	6,435	7,702	6,743
Sum	268,750	309,800	242,410

17.4 Hierarchical Clustering

With the development of multivariate statistic analysis, the clustering analysis method has been mature gradually and widely used in Biology, Economics, Sociology, Demography and so on. The hierarchical clustering is the most important method in clustering analysis. Its basic principle is that the two closest observations are joined to create a node by calculating the distance or similar coefficient between two observations. Subsequent nodes are created by pairwise joining of observations or nodes based on the distance between them, until all the nodes merge into a desired number of clusters. At the end, a tree structure can be created by retracing which items and nodes are merged [14].

In order to decide which clusters should be combined or where a cluster should be split, a measurement of dissimilarity between sets of observations is required. In most methods of hierarchical clustering, this can be achieved by using an appropriate metric (a measure of distance between pairs of observations) and a linkage criterion which specifies the dissimilarity of sets as a function of the pairwise distances of observations.

Some commonly used distance metrics for hierarchical clustering are the Euclid distance, Minkowski distance, City Block distance, Chebyshev distance, Mahal distance, Lance distance and Cosine similarity. The linkage criteria determines the distance between sets of observations as a function of the pairwise distances between observations. There are a variety of linkage criteria between clusters. Among them, three most popular ones are maximum or complete linkage, minimum or single linkage, mean or average linkage [15]. In our welding experiments, we defined the Euclid distance and the City Block distance as the distance metrics and took minimum linkage for hierarchical clustering. The expression of Euclid distance is

$$d_{ij}^{(2)} = \left(\sum_{t=1}^{p} \left| x_{it} - x_{jt} \right|^2 \right)^{1/2} \tag{17.12}$$

The expression of City Block distance is

$$d_{ij} = \left(\sum_{t=1}^{p} \left| x_{it} - x_{jt} \right| \right) \tag{17.13}$$

Mathematically, the minimum linkage is written as

$$D_{pq} = \min(d_{ij}) \quad x_i \in G_p, \quad x_j \in G_q \tag{17.14}$$

After the short-time Fourier transform, there were 36 groups of time frequency test data. The statistics method was used to extract the seven defined eigenvalues, then these eigenvalues were studied by clustering. The procedure of hierarchical clustering is as follows. First, the Euclid distance and the City Block distance were defined as the distance metrics, and the distance between observations were calculated. Second, the minimum linkage was used to create a tree structure. Finally, the discontinuous coefficients was set and the clustering tree was output. In this experiment, the discontinuous coefficients were 0.5, 0.7 and 0.9, respectively.

Totally $36 \times 2 \times 3 = 216$ groups of clustering data were obtained after calculation. The characteristics of clustering data was analyzed by drawing the clustering curves and curve-fittings. Using Bartlett-Hanning window whose length was 256 and step value was 5 for the short-time Fourier transform, and the Euclid distance, minimum linkage and discontinuous coefficient 0.9 for hierarchical cluster, it was found that the fluctuation trend of 6th fitting of clustering curve was similar to the 6th fitting curve of weld seam bead width. That means the 6th fitting of the clustering curve could reflect the weld bead width changing trend effectively. Figure 17.14 is the clustering curve based on the combination parameters mentioned above, the dotted line is the 6th fitting curve of clustering curve.

Figure 17.15 shows a 6th fitting curve of the clustering curve contrasting to the 6th fitting curve of weld seam bead. In Fig. 17.15, the dotted line is the weld bead width, the dot and dash line is the 6th fitting curve of weld bead width and the solid line is the 6th fitting curve of the clustering curve. It can be seen that the solid line and the dot and dash line have the consistent fluctuations. The 6th fitting curve of the clustering curve could reflect the weld bead width change trend effectively.

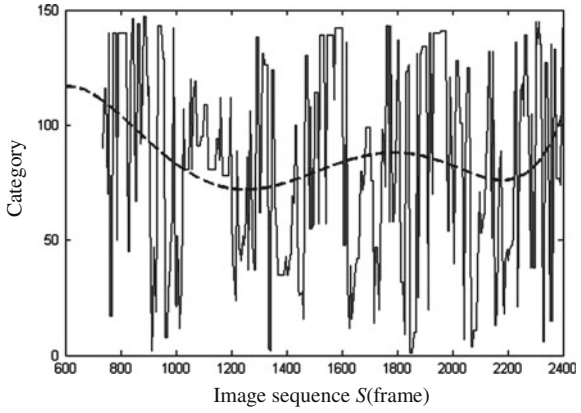

Fig. 17.14 Fitting *curve* of time–frequency clustering of metallic plume area

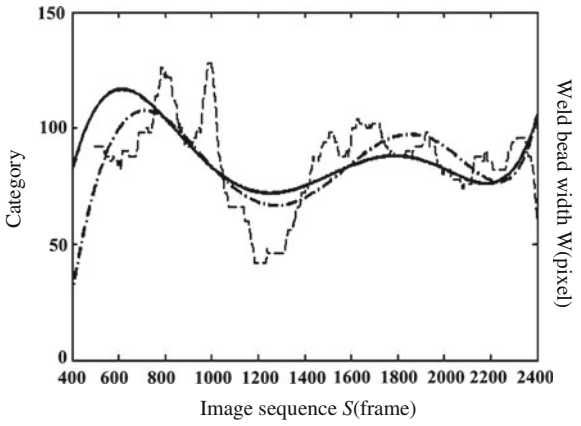

Fig. 17.15 Description of time–frequency clustering of area and weld bead width

Experimental results have shown that the weld bead width can be evaluated by using the time–frequency clustering of metallic plume area. It has provided a method to monitor and evaluate the welding quality in real time during disk laser welding by analyzing the time–frequency clustering of metallic plume area.

17.5 Conclusions

In a high power disk laser welding process, there exists a relation between the metallic plume area and the weld bead width. The metallic plume area could be calculated by using image processing techniques. It was found that the accurate plume area could be obtained by processing the plume images in the RGB color space and HSI color space.

The short-time Fourier transform could be applied to analyze the characteristics of plume area and extract the eigenvalues for the hierarchical clustering. Using the Bartlett-Hanning window whose length was 256 and step value was 5 for the short-time Fourier transform, and the Euclid distance, minimum linkage and discontinuous coefficient 0.9 for the hierarchical clustering, the 6th fitting curve of the clustering curve and the 6th fitting curve of weld bead width had the similar fluctuations. The 6th fitting of the clustering curve could reflect the weld bead width changing trend effectively. Experimental results showed that the time–frequency clustering of metallic plume area could be used to monitor and evaluate the welding quality during high power disk laser welding.

Acknowledgments This work is an expanded version of the paper published at WCECS 2012 in San Francisco, USA, October 24–26, 2012, and was supported in part by the National Natural Science Foundation of China under Grant 51175095, in part by the Guangdong Provincial Natural Science Foundation of China under Grants 10251009001000001 and 9151009001000020, and in part by the Specialized Research Fund for the Doctoral Program of Higher Education under Grant 20104420110001. Many thanks are given to Katayama Laboratory, Osaka University, Japan, for their assistance of laser welding experiments.

References

1. Khan MMA, Romoli L, Fiaschi M, Dini G, Sarri F (2011) Experimental design approach to the process parameter optimization for laser welding of martensitic stainless steels in a constrained overlap configuration. Opt Laser Technol 43(1):158–172
2. Katayama S, Kawahito Y, Mizutani M (2010) Elucidation of laser welding phenomena and factors affecting weld penetration and welding defects. Phys Procedia 5(Part B):9–17
3. Liu L, Chen M (2011) Interactions between laser and arc plasma during laser–arc hybrid welding of magnesium alloy. Opt Lasers Eng 49(9–10):1224–1231
4. Gao XD, Wang RL, Long GF, Katayama S (2012) Study of characteristics of plume based on hue-saturation-intensity during high-power disk laser welding. ACTA Physica Sinica, 61(14):148103-1-8
5. Khaleeq-ur-Rahman M, Siraj K, Rafique MS, Bhatti KA, Latif A, Jamil H, Basit M (2009) Laser induced plasma plume imaging and surface morphology of silicon. Nuclear Instruments Methods Phys Res B 267(7):1085–1088
6. Sibillano T, Anocona A, Berdi V, Lugara PM (2005) Correlation analysis in laser welding plasma. Opt Commun 251(1–3):139–148
7. Baik SH, Park SK, Kim CJ, Kim SY (2001) Holographic visualization of laser-induced plume in plused laser welding. Opt Laser Technol 33(1):67–70
8. Jiang P, Chen WZ, Guo J, Tian ZL (2001) The FFT Analyze of the acoustic signal on plasma in laser welding. Laser J 22(5):62–63
9. Molino A, Martina M, Vacca F, Masera G, Terreno A, Pasquettaz G, Angelo G (2009) FPGA implementation of time-frequency analysis algorithms for laser welding monitoring. Microprocessors Microsystems 33(3):179–190
10. Li G, Cai Y, WU Y (2009) Stability information in plasma image of high-power CO2 laser welding. Opt Lasers Eng 47(9):990–994
11. Gao XD, Wang RL, Yang YC (2012) Time-frequency characteristics clustering of metallic plume during high power disk laser welding, lecture notes in engineering and computer science. In: Proceedings of The world congress on engineering and computer science 2012, WCECS 2012, 24–26 Oct 2012, San Francisco, USA, pp 660–664
12. Wang X, Cheng P, Liang J (2011) Research of STFT time-frequency analysis algorithm and its application in train vibration analysis. Noise Vibr Control 31(1):65–68
13. Ge Z, Chen Z (2006) MATLAB time-frequency analysis technology and its application. Posts and Telecom Press, Beijing, pp 1–8
14. Du Z, Lin F (2004) A hierarchical clustering algorithm for MIMD architecture. Comput Biol Chem 28(5–6):417–419
15. Zhang Q, Zhang Y (2006) Hierarchical clustering of gene expression profiles with graphics hardware acceleration. Pattern Recogn Lett 27(6):676–681